

Quantum process tomography of unitary and near-unitary maps

Charles H. Baldwin, Amir Kalev, and Ivan H. Deutsch

Center for Quantum Information and Control, MSC07-4220, University of New Mexico, Albuquerque, New Mexico 87131-0001, USA

(Received 23 April 2014; published 17 July 2014)

We study quantum process tomography given the prior information that the map is a unitary or close to a unitary process. We show that a unitary map on a d -level system is completely characterized by a minimal set of d^2+d elements associated with a collection of POVMs, in contrast to the d^4-d^2 elements required for a general completely positive trace-preserving map. To achieve this lower bound, one must probe the map with particular sets of d pure states. We further compare the performance of different estimators inspired by compressed sensing, to reconstruct a near-unitary process from such data. We find that when we have accurate prior information, an appropriate compressed sensing method reduces the required data needed for high-fidelity estimation, and different estimators applied to the same data are sensitive to different types of noise. Convex optimization inspired by the techniques of compressed sensing can therefore be used both as indicators of error models and to validate the use of the prior assumptions.

DOI: [10.1103/PhysRevA.90.012110](https://doi.org/10.1103/PhysRevA.90.012110)

PACS number(s): 03.65.Wj, 03.67.—a

I. INTRODUCTION

The development of quantum information processing devices will require new diagnostic tools for efficiently characterizing errors and verifying performance. While standard quantum process tomography (QPT) was initially designed in order to characterize a “black box” [1]; in practice there is often substantial prior information about the intended target map that the device is designed to implement and various diagnostic experiments initially ensure that the device is performing well. Of particular importance is the design of devices whose target is a unitary map, e.g., quantum logic gates. Randomized benchmarking [2–4] is a scalable and robust technique that has been applied in many experiments, e.g., [5–10], in order to estimate the fidelity between the applied map and the target unitary. While such information is important, particularly for evaluating whether fault-tolerant error correction is possible, in practice we would like to learn more. Given a high-fidelity operation, to further improve performance it is critical to learn about and estimate the particular errors that led to a certain average error rate. It is therefore necessary to develop, along with benchmarking techniques, efficient QPT protocols beyond the “black box” model.

In the standard formulation of QPT, the applied process is an unknown completely positive, trace-preserving (CPTP) map, and therefore d^4-d^2 real numbers are required to completely characterize it [1]. If through, e.g., randomized benchmarking, we have high confidence that the applied map is close to a target unitary, we have substantial prior information. In this case, one may expect a dramatic reduction in the number of parameters, and hence resources, needed for reliable estimation of the full quantum process. Such reductions have been employed in the reconstruction of near-unitary process matrices describing linear optical networks [11,12]. Our goal in this work is to develop a general efficient protocol for QPT maps that are close to a target unitary map. Our focus is on establishing rigorous bounds on the minimal required resources and also on procedures to validate the use of prior knowledge.

Previous workers have studied methods to diagnose devices that are designed to implement target unitary maps. Recently, Reich *et al.* [13] showed that by choosing specially designed

sets of probe states, one can efficiently estimate the fidelity between an applied quantum process and a target unitary map. Moreover, Gutoskia and Johnston [14] showed that the measurement of $4d^2 - 2d - 4$ Pauli-like Hermitian (i.e., two-outcome) observables is sufficient to discriminate one unitary map from all other unitary maps, while identifying a unitary map from the set of all possible CPTP maps requires a measurement of $5d^2 - 3d - 5$ such observables. Utilizing prior information is important not only for efficiently gathering the required information, but also in designing the numerical estimators that reconstruct the process from the measured data. Such techniques, known as “compressed sensing” (CS), were originally introduced in the context of classical signal recovery [15]. Protocols inspired by these methods have been applied to QPT by Kosut and co-workers [16,17] and quantum state tomography (QST) by Gross *et al.* [18–20]. These procedures reliably approximate the process (or the state) in question and provide substantial reduction in the required data for this task.

In this work we further study the use of prior information to perform efficient QPT of maps close to unitary evolution and integrate this with convex optimization protocols inspired by CS techniques. Our results show two important features: (1) When we have accurate prior information, one can drastically reduce the required data needed for high-fidelity estimation. (2) Different estimators applied to the same data are sensitive to different types of noise. These estimators can, therefore, be used as indicators of error models and to validate (to some degree) the use of prior assumptions employed in the convex optimization.

After a brief review in Sec. II that serves to establish our notation for the various mathematical representations of quantum processes, in Sec. III we describe the mathematical tools that we use for QPT. Extending the results of Reich *et al.* [13] in Sec. IV, we present efficient procedures for QPT of unitary maps. In particular, we show that a given unitary map is fully characterized and completely distinguished from any other unitary map by a set of POVMs with a total minimum of $d^2 + d$ elements (measurement outcomes). This contrasts with previously known results [13,14]. To achieve this lower bound, one must probe the map with particular sets of d pure

states, and measure the evolved states with particular POVMs. Then, in Sec. V, we study how the methods for efficient characterization of perfect unitary maps, discussed in Sec. IV, could be utilized in physical scenarios where the applied map is close to a unitary map by formulating the reconstruction as a convex optimization problem. We examine the behaviors of different convex estimators based on correct or faulty prior information caused by noise, and use the results as a step towards validation of prior information and as a diagnosis of the nature of errors. We present our conclusions in Sec. VI.

II. REVIEW OF QUANTUM PROCESSES

There are different, equivalent, ways to represent a given quantum map. Among these are the well-known Kraus representation [21], process matrix representation [1], and Choi-Jamiołkowski isomorphism [22]. We briefly discuss the various representations in order to establish our notation. In the Kraus representation, a completely positive (CP) map \mathcal{E} is written as the sum

$$\mathcal{E}[\cdot] = \sum_{k=1}^K A_k [\cdot] A_k^\dagger, \quad (1)$$

where $[\cdot]$ represents the mathematical object on which the map acts, and $\{A_k\}$ are the Kraus operators. The map is trace preserving (TP) when $\sum_k A_k^\dagger A_k = 1$. The Kraus representation is not unique, and the number of independent, orthogonal, Kraus operators equals the rank of the map. If the map is unitary, $\mathcal{E}[\cdot] = U[\cdot]U^\dagger$, we have only one term in the above sum with $A_1 = U$.

The process matrix representation of a quantum map can be obtained from the Kraus representation of the map by writing the Kraus operators in a basis for complex matrices. Let Υ_n , $n = 1, \dots, d^2$ be an orthonormal basis for $d \times d$ complex matrices. Then by decomposing the Kraus operators as

$$A_k = \sum_{n=1}^{d^2} a_{nk} \Upsilon_n, \quad (2)$$

we obtain the process matrix representation of the map,

$$\mathcal{E}[\cdot] = \sum_{n,m=1}^{d^2} \chi_{nm} \Upsilon_m [\cdot] \Upsilon_n^\dagger. \quad (3)$$

The $d^2 \times d^2$ matrix χ , whose elements in the Υ_n basis are χ_{nm} , is the process matrix representation of the map. The CP constraint implies that the process matrix is a positive-semidefinite Hermitian matrix $\chi \geq 0$, $\chi = \chi^\dagger$. The process matrix of a TP map satisfies $\sum_{n,m} \chi_{nm} \Upsilon_m^\dagger \Upsilon_n = 1$. We say a map is pure if the process matrix is rank 1. A CP pure map is a unitary map if and only if it is a TP map.

The space of $d \times d$ complex matrices is a complex vector space of dimension d^2 , with inner product defined by

$$\langle\langle M_1 | M_2 \rangle\rangle = \text{Tr}(M_1^\dagger M_2) \quad (4)$$

(where we use a “double” bra-ket notation to indicate vectors in the corresponding d^2 -dimensional vector space). The process matrix χ can then be seen as an operator acting on a

d^2 -dimensional complex vector space,

$$\chi = \sum_{n,m=1}^{d^2} \chi_{nm} |\Upsilon_m\rangle\langle\langle \Upsilon_n|, \quad (5)$$

where $\langle\langle \Upsilon_m | \Upsilon_n \rangle\rangle = \delta_{n,m}$ is an orthonormal basis. In diagonal form,

$$\chi = \sum_{n=1}^{d^2} \lambda_n |V_n\rangle\langle\langle V_n|, \quad (6)$$

with eigenvalues λ_n and eigenvectors $|V_n\rangle$.

Finally, the Choi-Jamiołkowski representation is an isomorphism between a CP map on d -dimensional Hilbert space, $\mathcal{E}[\cdot]$, and a positive-semidefinite Hermitian operator acting on d^2 -dimensional tensor-product Hilbert space χ_c . According to the isomorphism,

$$\begin{aligned} \chi_c &= \sum_{n,m=1}^d |n\rangle\langle m|_A \otimes \mathcal{E}[|n\rangle\langle m|_B], \\ \mathcal{E}[\cdot] &= \text{Tr}_A \{ \chi_c ([\cdot]_A^\top \otimes 1_B) \}, \end{aligned} \quad (7)$$

with $\text{Tr}(\chi_c) = d$, and the superscript \top standing for the transpose. Being an operator on a d^2 -dimensional Hilbert space, χ_c has a representation as a $d^2 \times d^2$ matrix—the Choi matrix. The elements of the Choi matrix are then given by

$$(\chi_c)_{mknl} = \langle k | \mathcal{E}[|n\rangle\langle m|] | l \rangle, \quad (8)$$

where $m, k, n, l = 1, \dots, d$. The Choi matrix χ_c is an example of a process matrix, where the operator basis $\{\Upsilon_n\}$ appearing in Eq. (3) is the “standard” basis $\{\Upsilon_n = \Upsilon_{ij} = |i\rangle\langle j|\}$ with the relabeling of $n = 1, \dots, d^2$ by the pair ij with $i, j = 1, \dots, d$.

III. TOMOGRAPHY OF QUANTUM PROCESSES: THEORY AND NUMERICAL METHODS

QPT is the procedure by which one attempts to estimate a given process based on measurements made on the output of a well-chosen set of input states. Assuming for a moment the ideal, unphysical case that the collected data have neither statistical errors nor systematic, i.e., state preparation and measurement (SPAM) errors [23], then an informationally complete measurement record uniquely defines the map. Since any representation of a general map has $d^2(d^2 - 1)$ independent parameters, to specify the map one can, e.g., probe it with d^2 “input” states ρ_j^{in} which form a (Hermitian) operator basis. An informationally complete measurement on the output state specifies $d^2 - 1$ independent parameters of the map, $\rho_j^{\text{out}} = \mathcal{E}[\rho_j^{\text{in}}]$. We give two examples of such sets of states, which we will use below. The projection onto the d^2 kets,

$$|k\rangle, \quad k = 0, \dots, d-1,$$

$$\begin{aligned} &\frac{1}{\sqrt{2}}(|k\rangle + |n\rangle), \quad k = 0, \dots, d-2, \quad n = k+1, \dots, d-1, \\ &\frac{1}{\sqrt{2}}(|k\rangle + i|n\rangle), \quad k = 0, \dots, d-2, \quad n = k+1, \dots, d-1, \end{aligned} \quad (9)$$

forms an operator basis. These states are the generic states one typically considered in QPT protocols [1]. For powers of prime dimensions, the projection onto the d^2 kets,

$$\begin{aligned} &|n\rangle, \quad n = 0, \dots, d-1, \\ &|n; b\rangle, \quad b = 0, \dots, d-1, \quad n = 0, \dots, d-2, \end{aligned} \quad (10)$$

also forms an Hermitian operator basis. These vectors (together with $|d-1; b\rangle$, $b = 0, \dots, d-1$) are the elements that compose $d+1$ mutually unbiased bases (MUBs), with n labeling the vector in the b th basis [24]. Using either of these sets as input states and performing an informationally complete measurement on each output state completely specifies an arbitrary quantum map.

Consider an arbitrary measurement defined by a POVM with elements $\{E_l \geq 0\}$, with $\sum_l E_l = 1$. The probability of observing an outcome E_l for state ρ_j^{out} , $p_{jl} = \text{Tr}(\rho_j^{\text{out}} E_l)$, is expressed in terms of the process matrix using Eq. (3),

$$\begin{aligned} p_{jl} &= \text{Tr} \left(\sum_{n,m=1}^{d^2} \chi_{nm} \Upsilon_m \rho_j^{\text{in}} \Upsilon_n^\dagger E_l \right) \\ &= \sum_{n,m=1}^{d^2} D_{jlmn} \chi_{nm} = \text{Tr}(D_{jl}^\dagger \chi). \end{aligned} \quad (11)$$

Here $D_{jlmn} = \text{Tr}(\rho_j^{\text{in}} \Upsilon_n^\dagger E_l \Upsilon_m)$, a $d^2 \times d^2$ matrix. Alternatively, using Eq. (7) we can express p_{jl} in terms of the Choi matrix χ_c as

$$p_{jl} = \text{Tr}\{\chi_c((\rho_j^{\text{in}})^\top \otimes E_l)\}. \quad (12)$$

Comparing Eqs. (11) and (12) reveals that $D_{jl}^\dagger = (\rho_j^{\text{in}})^\top \otimes E_l$. Hence, the matrices D_{jl} allow us to relate the Choi matrix elements directly to the measurements statistics.

In practice, each measurement is repeated a finite number of times, and the measured data are comprised of frequencies of outcomes with finite statistical noise. We denote the frequency of the outcome E_l in measuring the state ρ_j^{out} by f_{jl} . Given the measured data, in order to characterize the quantum process in question, one must employ numerical estimators. We consider three estimation procedures: least squares (LS), ℓ_1 -norm CS (CS_{ℓ_1}), and Tr-norm CS (CS_{Tr}). The optimal solution for each of these estimators can be found using convex semidefinite programs (SDPs), given convex constraints $\chi \geq 0$ (CP constraint) and $\sum_{n,m} \chi_{nm} \Upsilon_m^\dagger \Upsilon_n = 1$ (TP constraint). We denote the estimated matrix returned by the procedures as $\hat{\chi}$. To solve the SDPs we use the MATLAB package CVX [25].

The LS estimator minimizes the (square of the) ℓ_2 -norm distance between the measurement record (consisting of frequencies) and the expected measurement record,

$$\begin{aligned} &\min \sum_{j,l} |f_{jl} - \text{Tr}(D_{jl}^\dagger \chi)|^2 \\ &\text{subject to} \sum_{n,m} \chi_{nm} \Upsilon_m^\dagger \Upsilon_n = 1, \\ &\chi = \chi^\dagger, \quad \chi \geq 0. \end{aligned} \quad (13)$$

The estimated matrix $\hat{\chi}$ is the (constrained) maximum-likelihood solution under the assumption that the data are

drawn from a Gaussian distribution. The LS program makes no prior assumptions about the nature of the process matrix we are attempting to reconstruct (besides being a CPTP process).

The next two procedures are inspired by CS in classical signal processing [26,27]. Often, when we are attempting to estimate a process matrix, we have some prior knowledge about the physics of the device that implements the map. Incorporating this knowledge into our numerical procedure may result in an efficient estimation technique. This, however, makes the method biased towards process matrices that satisfy our assumptions. Hence, if we made a wrong assumption about the implemented process, the procedure can report an estimate that could have poor fidelity with the applied process. In this case the estimation procedure fails. We will return to this problem later. For now we discuss two main convex methods for quantum process estimation, with roots in CS.

The original CS estimation technique [15] is based on the assumption that the optimization variable (in our case, the process matrix) is a sparse vector in a known representation. When this is the case the optimization variable can be much more efficiently extracted by minimizing its ℓ_1 -norm [26]. To use this method efficiently for the problem of QPT, the process matrix should thus be close to a sparse matrix in a known basis [16]. In an application such as the implementation of a quantum logic gate, one is attempting to build a target unitary map U_t . We therefore expect that if the error in implementation is small, when expressed in an orthogonal basis $\{V_n\}$ that includes the target process as a member, $V_1 = U_t$, the process matrix describing the applied map will be close to a sparse matrix. This in turn implies that the CS_{ℓ_1} optimization algorithm can efficiently estimate the applied process.

We thus define the CS_{ℓ_1} estimator as follows:

$$\begin{aligned} &\min \|\chi\|_1 \\ &\text{subject to} \sum_{j,l} |f_{jl} - \text{Tr}(D_{jl}^\dagger \chi)|^2 \leq \varepsilon, \\ &\sum_{n,m} \chi_{nm} V_m^\dagger V_n = 1, \\ &\chi = \chi^\dagger, \quad \chi \geq 0, \end{aligned} \quad (14)$$

where here the matrices D_{jl} are represented in the $\{V_n\}$ basis, $D_{jlmn} = \text{Tr}(\rho_j^{\text{in}} V_n^\dagger E_l V_m)$. The first constraint equation now requires that the probabilities from our optimization variable should match our measurement frequencies up to some threshold ε . The threshold is chosen based on a physical model of the statistical noise sources for the measurements.

In the numerical simulation to be studied in Sec. V, assuming a target unitary map U_t without loss of generality, we take the basis $\{V_n\} = \{U_t, U_t \Upsilon_2, U_t \Upsilon_3, \dots, U_t \Upsilon_n\}$, where $\{\Upsilon_n\}$ is the generalized Gell-Mann basis. We can regard the representation of the applied process matrix in this basis as a transformation into the ‘‘interaction picture’’ with respect to the target map; any deviation of the applied process matrix from the projection onto $|U_t\rangle$ indicates an error. Therefore the CS_{ℓ_1} directly estimates the error matrix studied in detail in [28]. This feature holds also if the target map is not a unitary map. Representing the applied map in the eigenbasis of the target map results in an error matrix; the latter is approximated by the CS_{ℓ_1} procedure.

The second type of CS-inspired estimation technique we study is based on the prior assumption that the process matrix is close to a low-rank matrix. This is equivalent to the assumption that the process is close to a (possibly unknown) unitary map. It was shown in [27] that one can complete a low-rank matrix M , for which we have only partial information, by minimizing its nuclear norm $\|M\|_* = \text{Tr}\sqrt{M^\dagger M}$. This procedure has been applied to QST [19,20,29,30], for states close to pure states, and thus close to low-rank density matrices ρ . Because $\rho \geq 0$, $\|\rho\|_* = \|\rho\|_{\text{Tr}} = \text{Tr}(\rho)$. We thus refer to this procedure as CS_{Tr} .

For QPT we take a similar approach. Since our optimization variable is the process matrix χ , which is positive semidefinite, as in QST, $\|\chi\|_* = \text{Tr}(\chi)$. Typically, the trace of the process matrix is part of the TP constraint equations, as for example in the CS_{ℓ_1} estimator. In the current procedure, however, we must drop any equation that constrains the trace of the process matrix. To deal with this and maintain the maximal number of constraint equations, we take an operator basis of traceless Hermitian matrices, thereby ensuring that there is only one equation relevant to the trace of the process matrix, which is dropped as a constraint. We thus define the CS_{Tr} estimator as follows:

$$\begin{aligned} & \min \text{Tr}(\chi) \\ & \text{subject to } \sum_{j,l} |f_{jl} - \text{Tr}(D_{jl}^\dagger \chi)|^2 \leq \varepsilon, \\ & \sum_{n,m \neq 1} \chi_{nm} \Upsilon_m^\dagger \Upsilon_n = 0, \\ & \chi = \chi^\dagger, \chi \geq 0, \end{aligned} \quad (15)$$

where now χ and D_{jl} are represented in a basis with $\Upsilon_1 = 1$ and the elements $\Upsilon_{m \neq 1}$ are orthogonal traceless Hermitian matrices. The sum in the second constraint includes all the terms except $n = m = 1$. While the CS_{Tr} estimator is basis independent, our numerical analysis indicates that this choice of basis improves the performance. Also, as in the CS_{ℓ_1} procedure, we constrain the probabilities based on the optimization variable to match our measured frequencies up to some threshold ε , determined by our knowledge of the statistical noise. Finally, the estimated process matrix $\hat{\chi}$ should be renormalized such that $\text{Tr}(\hat{\chi}) = d$.

IV. TOMOGRAPHY OF A UNITARY PROCESS

A. Minimal sets of probes and measurements

To begin, we consider the most basic problem—QPT of a unitary map. Here we treat the idealized limit where the measurement record has neither statistical errors nor systematic errors. In doing so we establish the mathematical relationships that determine the minimal set of input states and POVM elements required for perfect QPT of a unitary map. We return to the question of statistical errors in the following section.

In a recent work, Reich *et al.* [13] developed an algebraic framework to identify sets of input states from which one can discriminate any two unitary maps given the corresponding output states. In particular, a set of input states $\{\rho_j^{\text{in}}\}$ provides sufficient information to discriminate any two unitary maps

if and only if the identity operator is the only operator that commutes with all ρ_j^{in} 's in this set. We call such a set of states “unitarily informationally complete” (UIC) set. More generally, under unitary evolution, the output states $\{\rho_j^{\text{out}} = U\rho_j^{\text{in}}U^\dagger\}$ completely distinguishes U from any other CPTP map if and only if $\{\rho_j^{\text{in}}\}$ is a UIC set.

An example of such a set on a d -level system is

$$\mathcal{S} = \left\{ \rho_0^{\text{in}} = \sum_{n=0}^{d-1} \lambda_n |n\rangle\langle n|, \rho_1^{\text{in}} = |+\rangle\langle +| \right\}, \quad (16)$$

where the eigenvalues of ρ_0^{in} are nondegenerate, $\{|n\rangle\}$ is an orthonormal basis for the Hilbert space, and $|+\rangle = \sum_{n=0}^{d-1} |n\rangle/\sqrt{d}$. Reich *et al.* [13] considered \mathcal{S} in order to set numerical bounds on the average fidelity between a specific unitary map and a random CPTP map. In fact, \mathcal{S} is a UIC set with the minimal number of input states required for complete QPT of a unitary map on a d -dimensional Hilbert space.

To see this, we write the unitary map as a transformation from the orthonormal basis $\{|n\rangle\}$ to its image basis $\{|u_n\rangle\}$,

$$U = \sum_{n=0}^{d-1} |u_n\rangle\langle n|. \quad (17)$$

In its essence, the task in QPT of a unitary map is to fully characterize the basis $\{|u_n\rangle\}$, along with the relative phases of the summands $\{|u_n\rangle\langle n|\}$. By probing the map with ρ_0^{in} , we obtain the output state $\rho_0^{\text{out}} = U\rho_0^{\text{in}}U^\dagger = \sum_{n=0}^{d-1} \lambda_n |u_n\rangle\langle u_n|$, which we fully characterize by means of an informationally complete POVM. Such a POVM has at least $d^2 - 1$ elements. We then diagonalize ρ_0^{out} and learn $\{|u_n\rangle\langle u_n|\}$. Without loss of generality, we take the global phase of $|u_0\rangle$ to be zero. Next, we probe the map with ρ_1^{in} , and fully characterize the output state $\rho_1^{\text{out}} = \sum_{n,m=0}^{d-1} |u_n\rangle\langle u_m|/d$ with an informationally complete POVM. The $\{|u_n\rangle\}$ are calculated according to the relation $|u_n\rangle\langle u_n|\rho_1^{\text{out}}|u_0\rangle = |u_n\rangle/d$. This procedure identifies a unique orthonormal basis $\{|u_n\rangle\}$ if and only if the map is a unitary map.

So far we have not specified the nature of the “informationally complete measurement on the output state.” Under a unitary evolution ρ_1^{out} is a pure state. To fully characterize it, we may therefore use a measurement that is informationally complete for pure states. Flammia *et al.* [31] showed that the 2d operators

$$\begin{aligned} E_0 &= a|0\rangle\langle 0|, \\ E_n &= b(1 + |0\rangle\langle n| + |n\rangle\langle 0|), \quad n = 1, \dots, d-1, \\ \tilde{E}_n &= b[1 + i(|0\rangle\langle n| - |n\rangle\langle 0|)], \quad n = 1, \dots, d-1, \\ E_{2d} &= 1 - \left[E_0 + \sum_{n=1}^{d-1} (E_n + \tilde{E}_n) \right] \end{aligned} \quad (18)$$

with a and b chosen such that $E_{2d} \geq 0$ represent an informationally complete POVM for pure states with the minimal number of outcomes. That is, all pure states in a d -dimensional Hilbert space (except those in a set of measure zero [32]) are completely determined by the probabilities of these POVM elements. The total minimal number of POVM elements that are needed for complete characterization of a unitary map using the above procedure is thus $d^2 - 1 + 2d$.

While \mathcal{S} is the minimal UIC set, in practice we do not have reliable procedures to produce a desired, reproducible, mixed state ρ_0^{in} . We thus turn our attention to minimal UIC sets that are composed only of pure states (arbitrary pure states can be reliably produced using the tools of quantum control [9]). Such UIC sets are composed of d pure states that form a nonorthogonal vector basis for the d -dimensional Hilbert space. For example, the set

$$\begin{aligned} |\psi_n\rangle &= |n\rangle, \quad n = 0, \dots, d-2, \\ |\psi_{d-1}\rangle &= |+\rangle = \frac{1}{\sqrt{d}} \sum_{n=0}^{d-1} |n\rangle, \end{aligned} \quad (19)$$

a subset of the states of Eq. (10), is a minimal UIC set of pure states. A similar set (with $d+1$ elements) was considered in [13]. Here we focus on a different set of d pure states that is UIC,

$$\begin{aligned} |\psi_0\rangle &= |0\rangle, \\ |\psi_n\rangle &= \frac{1}{\sqrt{2}}(|0\rangle + |n\rangle), \quad n = 1, \dots, d-1. \end{aligned} \quad (20)$$

This is a subset of the standard states used in QPT, Eq. (9). The only operator that commutes with all of the projectors $\{|\psi_n\rangle\langle\psi_n|\}$, $n = 0, \dots, d-1$, is the identity operator.

A generic tomographic procedure for a unitary process using the set given in Eq. (20) can be described as follows. First let the map act on $|\psi_0\rangle$ and make an informationally complete measurement on the output state $U|\psi_0\rangle = |u_0\rangle$, from which we can obtain the state $|u_0\rangle$ (up to a global phase that we can set to zero). Next, let the unitary map act on $|\psi_1\rangle$ and perform an informationally complete measurement on the output state $U|\psi_1\rangle\langle\psi_1|U^\dagger$. From the relation $U|\psi_1\rangle\langle\psi_1|U^\dagger|u_0\rangle = \frac{1}{2}(|u_0\rangle + |u_1\rangle)$ we obtain the state $|u_1\rangle$, including its phase relative to $|u_0\rangle$. We repeat this procedure for every state $|\psi_n\rangle$ with $n = 1, \dots, d-1$, thereby obtaining all the information about the basis $\{|u_n\rangle\}$, including the relative phases in the sum of Eq. (17), and completing the tomography procedure for a unitary map. In this protocol, because input and output states are ideally pure, we may use the POVM of Eq. (18), which has $2d$ measurement outcomes, as the informationally complete measurement on each output state. We thus conclude that the total number of POVM elements needed for reconstruction of a unitary map based on the protocol above is $d \times 2d = 2d^2$. This is the minimal number of measurement outcomes required to distinguish a unitary map from an arbitrary CPTP map, when the map is probed with pure input states.

While $2d^2 > d^2 - 1 + 2d$, the total number of measurement outcomes required for the minimal (mixed) UIC set \mathcal{S} , by using a UIC set of d pure states, we can fully distinguish a unitary map from the set of all unitary maps by measuring sets of POVMs that have in total only $d^2 + d$ elements. The key ingredient is to note that in the procedure above, we have not used the orthogonality of the basis $\{|u_n\rangle\}$. By taking this into account, we can reduce the number of required measurement outcomes on each output state. The first step is, as before, to use $|\psi_0\rangle$ as a probe state and perform an informationally complete measurement, which has $2d$ outcomes, on the output state $|u_0\rangle$. From this measurement we determine $|u_0\rangle$ completely

(up to an irrelevant global phase). Note that the probability of detecting the outcome E_0 is

$$p_{00} = \langle u_0|E_0|u_0\rangle = a|c_{00}|^2, \quad (21)$$

and since the amplitude c_{00} can be taken to be positive without loss of generality, we deduce that $c_{00} = \sqrt{p_{00}/a}$. Similarly, from the probabilities of the outcomes E_n and \tilde{E}_n we obtain the real and imaginary parts of c_{0n} , respectively,

$$\begin{aligned} p_{0n} &= \langle u_0|E_n|u_0\rangle = b[1 + 2c_{00}\text{Re}(c_{0n})], \\ \tilde{p}_{0n} &= \langle u_0|\tilde{E}_n|u_0\rangle = b[1 + 2c_{00}\text{Im}(c_{0n})]. \end{aligned} \quad (22)$$

Thus, we obtain full information about the state $|u_0\rangle$. This procedure fails for states with $c_{00} = 0$, a set of measure zero. Next, we probe the unitary map with $|\psi_1\rangle$ of Eq. (20), and perform an informationally complete measurement on the output state $\frac{1}{\sqrt{2}}(|u_0\rangle + |u_1\rangle)$. However, since $|u_1\rangle$ is orthogonal to $|u_0\rangle$, it is sufficient to make a measurement that yields only the first $d-1$ probability amplitudes $c_{1n} = \langle n|u_1\rangle$, $n = 0, \dots, d-2$, and then use the orthogonality condition $\langle u_0|u_1\rangle = \langle u_1|u_0\rangle = 0$ to calculate the d th amplitude c_{1d-1} . A measurement with $2d-2$ outcomes can be, for example, the measurement of Eq. (18), but with $n = 0, \dots, d-2$. Therefore, to measure the state $|u_k\rangle$, $k = 0, \dots, d-1$, we perform a measurement with $2d-2k$ outcomes, and use $2k$ orthogonality relations.

Overall, if we have prior information that the map is unitary, this protocol shows that we can reconstruct it from $d^2 + d$ measurement outcomes. This number is, by construction, the minimum number of POVM elements required to reconstruct a unitary map. Although this protocol is slightly more efficient than the previous one, it assumes much more. Crucially, the former protocol assumes *no prior knowledge of the map* and can be cast as a convex optimization program to uniquely reconstruct an applied unitary map after informationally complete measurements on d input pure states. This feature makes it useful for laboratory implementation, when estimating an applied map from measured data.

B. Simulating tomography of a unitary process

To study the behavior of the reconstruction using the UIC sets of pure states discussed above, in this section we simulate QPT based on the LS estimator Eq. (13). Here, and throughout, we consider a target unitary map on a qudit of dimension $d = 5$, a Hilbert space dimension sufficient to test the general performance of the estimators. We generate a random process matrix and let it act on a preassigned set of input states. We then use an informationally complete measurement on the output states to generate the expected probability distribution according to Eq. (12). Finally, we simulate the measurement record by the outcome probabilities plus a Gaussian-distributed random variable W_{jl} with mean zero and variance 1,

$$f_{jl} = p_{jl} + \sigma W_{jl}. \quad (23)$$

The magnitude σ is held constant for all j and l . In this way, by repeating the measurement many times, the frequencies are normal Gaussian-distributed random variables with mean

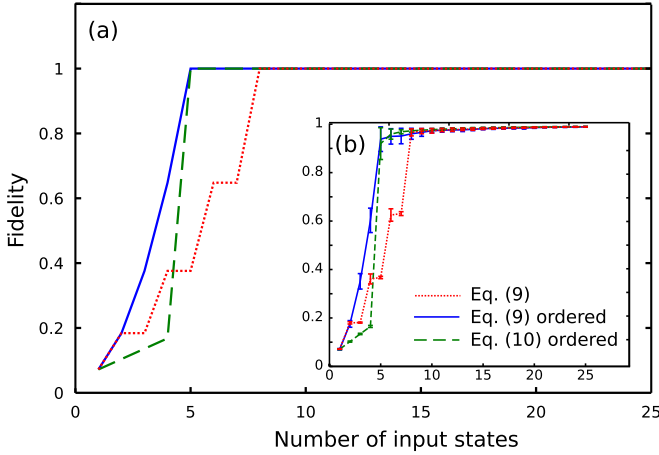


FIG. 1. (Color online) Fidelity between a unitary map on a ($d = 5$)-dimensional Hilbert space and the LS estimate of the process matrix (averaged over 50 Haar-random unitary maps) as a function of the number of input states in the absence (a) and in the presence (b) of statistical noise. The error bars represent the standard deviation. The data represented in the dotted (red) line are obtained from an informationally complete measurement on the states produced by applying the unitary map to all d^2 input states in the order specified in Eq. (9). In the solid (blue) line the first five input states are those of Eq. (20), and the remaining states are chosen from Eq. (9) in an arbitrary order. In the dashed (green) line the first five input states are those of Eq. (19) and the remaining state from Eq. (10). Unit fidelity is obtained after $d = 5$ input states in a UIC set. In the presence of statistical error, as seen in (b), the main features of the fidelity remain qualitatively the same—by choosing the correct set of input states we obtain a reliable reconstruction after d input states, up to statistical error. The statistical fluctuations in the data are modeled by Eq. (23), a normal distribution, with $\sigma = 10^{-4}$.

given by the probability p_{jl} and variance describing the noise of large but finite counting statistics.

To evaluate the performance of the estimators, we calculate the (Uhlmann) fidelity between the reconstructed process matrix $\hat{\chi}$ and the process matrix of a target unitary map $\chi_t = |U_t\rangle\rangle\langle\langle U_t|$,

$$F(\hat{\chi}, \chi_t) = \frac{1}{d^2} \left(\text{Tr} \sqrt{\sqrt{\hat{\chi}} \chi_t \sqrt{\hat{\chi}}} \right)^2 = \frac{1}{d^2} \langle\langle U_t | \hat{\chi} | U_t \rangle\rangle \quad (24)$$

as a function of the number of input states. By this we mean that we simulate an estimator that uses all of the data derived by inputting the first $k \leq d$ states in a particular order and measuring the output states with an informationally complete POVM. The input states are taken to be those of Eqs. (9) and (10). As we are considering the ideal case of a perfect unitary map, each output state is measured with the informationally complete measurement for pure states of Eq. (18).

To begin, we treat the idealized situation where there is no noise in the data, i.e., $\sigma = 0$ in Eq. (23). We clearly see in Fig. 1(a) that the order in which one uses the input states affects the way in which we gain information about the process. In the dotted (red) line we use the generic order of input states used for general process tomography given in Eq. (9) starting with $k = 0$ and running over n . The plateaus in the plot indicate

that we gain information only from particular states in that set, while others do not provide additional information. The positions of the plateaus occur for the same input state for each of the sampled unitary maps, and they are independent of their details. To see this point more clearly, take for example the two input states with $k = 0$ and $n = 1$ of Eq. (9), $\frac{1}{\sqrt{2}}(|0\rangle + |1\rangle)$ and $\frac{1}{\sqrt{2}}(|0\rangle + i|1\rangle)$. Probing a unitary map with these two states gives us the same information, namely, the image $|u_1\rangle$. Since probing the unitary map with either state gives the same information, for efficient reconstruction it is sufficient to probe the map only with one of the states. Therefore, to obtain an efficient reconstruction of a unitary map with $d = 5$ pure input states, the latter must form a UIC set. Such states are used in the solid (blue) line and the dashed (green) line in Fig. 1. In the solid line we input the first $d = 5$ input states in Eq. (20) and then the remainder of the states of Eq. (9). In the dashed line, on the other hand, the first five input states are those of Eq. (19), followed by the remainder of the states of Eq. (10). Note that in our LS program, for the reconstruction of the process matrix, we did not assume any structure on the reconstructed map except that it is a CPTP map. Yet, after d input states of Eq. (20) or Eq. (19), the LS estimator returns the target map. Thus, d input states are sufficient to completely identify a unitary map among *all* CPTP maps.

Because we assumed a (nonphysical) hypothetical situation where there is no noise in the data, the fidelity between the reconstructed map and the target map eventually reaches unity. In any physical implementation, however, even in the absence of any systematic errors, finite sampling always results in statistical noise. Qualitatively, such noise does not affect the key features of the results above in the large-sampling (Gaussian-noise) limit, as seen in Fig. 1(b). The effect of the statistical noise on the fidelity between the estimate and the target map is twofold: it reduces its maximal value below 1 (depending on the level of noise), and after d input states, the plateau in the fidelity acquires a shallow slope.

The addition of some statistical noise to the measurement record still allows us to obtain, more or less, all the information about the process with d input states; if the map itself is far from unitary, the reconstruction can fail dramatically. We address this behavior and methods to validate prior assumptions in the next section.

V. TOMOGRAPHY OF A NEAR-UNITARY PROCESS

While the previous section established the behavior of the LS estimator in the situation that the applied map was equal to the target unitary map, in any physical implementation this is never exactly true. Our goal is to understand how well the idealized case considered above carries over to the realistic case under the assumption that the errors in implementation are sufficiently small. Moreover, we seek to *validate* the prior assumptions that are used in the protocol and to use the estimation procedures to *characterize* the kinds of errors that lead to imperfections in the applied map.

Let us denote the target unitary process \mathcal{E}_t with corresponding process matrix χ_t . Due to experimental imperfections, the process actually being implemented is \mathcal{E}_a , with corresponding process matrix χ_a . We assume good experimental control so

that the implementation errors are low, and hence χ_a is close to χ_t . Our goal is to reconstruct χ_a as faithfully as possible in order to diagnose the errors that led to the creation of \mathcal{E}_a .

We consider two types of imperfections in the implementation of the map: ‘‘coherent’’ and ‘‘incoherent’’ errors. A coherent error is one where the applied map is also unitary, but ‘‘rotated’’ from the target. We define incoherent errors as errors that are not coherent errors, for example, statistical mixtures of different unitary maps arising from inhomogeneous control or decoherence.

Under the assumption that the applied process is close to a known target unitary map, we expect the resource reduction obtained in the ideal case, where there were no implementation errors, to carry over here to the noisy case. We thus study the performance of the estimators probed with states that are efficient for reconstruction of a unitary map, e.g., the states of Eq. (20). Moreover, using the knowledge that χ_a is close to χ_t , we expect that in the eigenbasis of χ_t , χ_a is close to a sparse matrix, and we therefore expect the CS_{ℓ_1} procedure to yield an estimate $\hat{\chi}$ with high fidelity with χ_a with very little data. In addition, since the CS_{Tr} estimator performs well when estimating process matrices that are close to low-rank matrices, when the target map χ_t is a unitary map, and χ_a is close to χ_t , we expect that the CS_{Tr} estimator should return an estimate with high fidelity to χ_a after input of d UIC states.

In some cases, however, our assumption that χ_a is close to χ_t is flawed. Then these estimation procedures will in general return an estimate $\hat{\chi}$ that is very different from χ_a . In what follows we will see that one can utilize the sensitivity of the estimators to the prior assumptions as an indicator for the possible types of errors that occurred in the implementation of the map, and to validate, to some degree, whether prior assumptions are justified.

As in Sec. IV, in the numerical simulations below we consider the estimation of random maps on a ($d = 5$)-dimensional Hilbert space. We ignore SPAM errors, assuming that the input states are perfectly prepared and that the output states are perfectly measured (up to statistical errors) with informationally complete measurement of the MUB. The target map \mathcal{E}_t is a Haar-random unitary map, and the applied map is generated by its composition with a map that describes the error channel, $\mathcal{E}_a = \mathcal{E}_{\text{err}} \circ \mathcal{E}_t$. For coherent errors, we take $\mathcal{E}_t[\cdot] = U_t[\cdot]U_t^\dagger$ and $\mathcal{E}_{\text{err}}[\cdot] = U_{\text{err}}[\cdot]U_{\text{err}}^\dagger$, where $U_{\text{err}} = e^{i\eta H}$, with $\eta \geq 0$, and H is a random Hermitian matrix selected by the Hilbert-Schmidt measure. For incoherent errors we consider the case where

$$\mathcal{E}_{\text{err}}[\cdot] = (1 - \xi)[\cdot] + \xi \sum_{n=1}^{d^2} A_n[\cdot]A_n^\dagger, \quad (25)$$

so that the applied map is given by

$$\mathcal{E}_a[\cdot] = (1 - \xi)U_t[\cdot]U_t^\dagger + \xi \sum_{n=1}^{d^2} A_n U_t[\cdot]U_t^\dagger A_n^\dagger. \quad (26)$$

The set $\{A_n U_t\}$ are Kraus operators associated with a CP map. Equation (26) can be interpreted as a mixture of two maps—the target map and an error-related map, with a mixing parameter $\xi \in [0, 1]$. The $\{A_n\}$'s are generated by choosing a Haar-random a unitary matrix U of dimension d^3 , and a

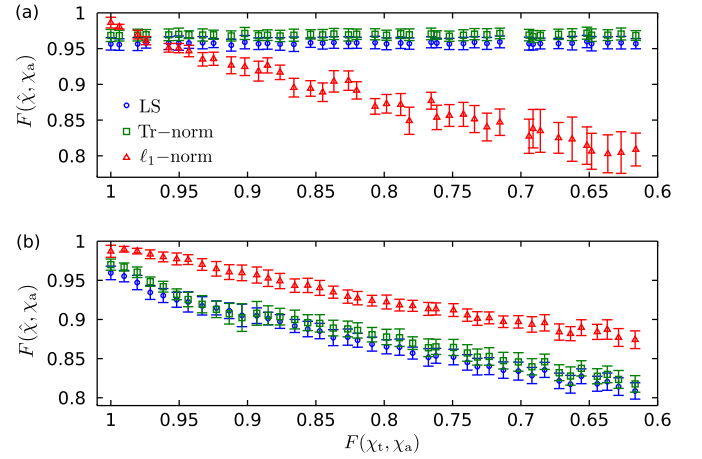


FIG. 2. (Color online) The fidelity between the estimate and the applied map as a function of the fidelity between the target map and the applied map for the case of coherent (a) and incoherent (b) errors. The error bars represent the standard deviation. The estimates are obtained with data from only the five UIC input states of Eq. (20). Each data point in the plots is obtained by an average over 50 random target unitary maps each with a random error map. (a) Coherent errors: The applied map is given by $U_a = U_{\text{err}}U_t$, where U_t is a Haar-random unitary map, $U_{\text{err}} = e^{i\eta H}$, $\eta \in [0, 3]$, and H is a random Hermitian matrix selected by the Hilbert-Schmidt measure, normalized to $\text{Tr}H = 1$. While the fidelities of the estimator based on the CS_{Tr} and the LS minimizations remain more or less constant, the fidelity of the estimator based on the CS_{ℓ_1} minimization decreases as the fidelity between the applied and the target maps decreases. This is an indicator of the sensitivity of CS_{ℓ_1} to coherent errors. (b) Incoherent errors: The applied map is given by Eq. (26). The numerical simulation was done by choosing at random values of ξ from a uniform distribution on $[0, 0.6]$. For each value we generated Haar-random unitary target maps U_t and 25 randomly selected Kraus operators from the Hilbert-Schmidt measure as prescribed in Ref. [34]. The estimate based on the CS_{ℓ_1} minimization performs better than the estimate based on the CS_{Tr} and the LS minimization procedures, and thus, the CS_{ℓ_1} estimator is more robust to incoherent errors of the form of Eq. (26) than either the CS_{Tr} or the LS estimator.

random pure state of dimension d^2 from the Hilbert-Schmidt measure $|v\rangle$ such that $A_n = \langle n|U|v\rangle$ where the set $\{|n\rangle\}$ is a computational basis [34].

We first test the sensitivity of the CS_{ℓ_1} , CS_{Tr} , and LS estimators to the error type and magnitude. In Fig. 2 we plot the fidelity between the applied matrix χ_a and the reconstructed matrices $\hat{\chi}$ determined by each of the three estimators, as a function of the fidelity between the applied process χ_a and the target χ_t . The latter fidelity $F(\chi_t, \chi_a)$ is a measure of the magnitude of the error in the applied process. Each data point is obtained by an average of 50 random error processes [Fig. 2(a) for coherent errors and Fig. 2(b) for incoherent errors] based on informationally complete measurements from $d = 5$ UIC input states. As expected, all of the estimators return reconstructions that have high fidelity with the applied map when the applied map is close to the target unitary map $\mathcal{E}_a[\cdot] \approx U_t[\cdot]U_t^\dagger$. In particular in our simulations $F(\hat{\chi}, \chi_a) \gtrsim 0.95$ when $F(\chi_t, \chi_a) \gtrsim 0.97$.

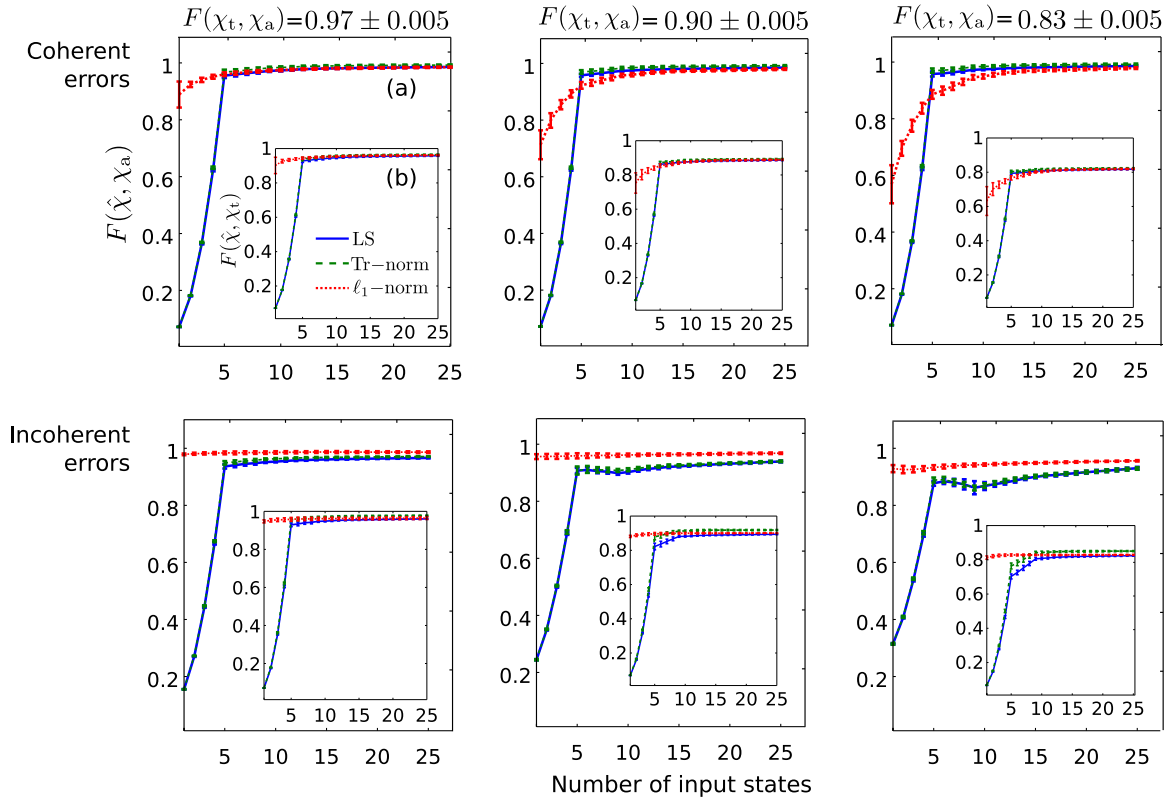


FIG. 3. (Color online) The fidelity between the estimate and the applied map, $F(\hat{\chi}, \chi_a)$ (a), and the estimate and the target map, $F(\hat{\chi}, \chi_t)$, inset (b), as a function of the number of input states, averaged over 50 applied processes, using different estimators, and under different error models for the applied map. Error bars represent the standard deviation. Each column corresponds to a different magnitude of implementation error, represented by the fidelity between the applied and target maps $F(\chi_t, \chi_a)$. Top row: Coherent errors as in Fig. 2(a). For a low error magnitude $F(\chi_t, \chi_a) = 0.97 \pm 0.005$, the three estimators return a high-fidelity estimate with the applied and the target maps. The CS_{ℓ_1} estimator returns a reliable estimate with the information obtained from a single input state, while the CS_{Tr} and the LS minimization procedures reliably estimate the map after five UIC input states. The CS_{Tr} and the LS estimators are robust to coherent error and perform essentially the same as the error level increases; here, $F(\chi_t, \chi_a) = 0.90 \pm 0.005$ and $F(\chi_t, \chi_a) = 0.83 \pm 0.005$. A noticeable slope in the fidelity as a function of the number of input states for the CS_{ℓ_1} estimator, and a sharp kink in this curve for the LS and CS_{Tr} estimators, are indicators of the coherent-error type. Bottom row: Incoherent errors as in Fig. 2(b). The CS_{ℓ_1} estimator returns a reliable estimate with information for higher error magnitudes; here, $F(\chi_t, \chi_a) = 0.90 \pm 0.005$ and $F(\chi_t, \chi_a) = 0.83 \pm 0.005$ with the fidelity relatively constant after a single input state. In contrast, the CS_{Tr} and the LS estimators are more sensitive to an increase in the magnitude of incoherent errors. As the error level increases, the sharp transition in the fidelity as a function of the number of input states becomes smoother as the noise increases. These features of the fidelity curves for the three estimators are indicators of the incoherent-error type.

However, as the implementation error increases and $F(\chi_t, \chi_a)$ decreases, the performance of the three estimators depends strongly on the nature of the errors. The CS_{ℓ_1} is more sensitive to coherent errors than the CS_{Tr} and LS estimators, as seen in Fig. 2(a). Using the data from $d = 5$ UIC input states, the fidelity between the CS_{ℓ_1} estimate and the applied map begins to fall below $\sim 90\%$ in these simulations for $F(\chi_t, \chi_a) \lesssim 0.9$ while the CS_{Tr} and LS estimators maintain their high fidelity. This trend is reversed for incoherent errors, as seen in Fig. 2(b). The CS_{ℓ_1} estimator is more robust to incoherent errors of the form of Eq. (26) than either the CS_{Tr} or LS estimator because the process matrix is no longer close to a low-rank matrix, but it is still relatively close to a sparse matrix in the preferred basis. As the incoherent-error magnitude increases, the CS_{ℓ_1} method returns an estimate with (on average) higher fidelity with the applied map than either the CS_{Tr} or the LS estimate. We thus conclude that when the applied map is sufficiently far from the target unitary map, the

performance of the three estimators varies in a manner that depends on the type of the error, and we can use this variation as an indicator of the type of error that occurred in the applied process.

To understand the validation and diagnosis protocol, we study the fidelity between the estimate and the applied map [Fig. 3(a)] and between the estimate and the target map [Fig. 3(b)] as a function of the number of input states, as studied previously in Sec. IV. We plot the fidelity averaged over 50 Haar-random applied maps. The estimator based on the ℓ_1 -norm is somewhat unstable when the reconstruction is based on data taken from very few input states. To overcome this instability, one can use the same data obtained from the first d input states, in different orders, to estimate the process, and then average over the resulting processes. This reduces the sensitivity to the specific choice of state of the first input state. In Fig. 3 we have used such averaging for estimating the process based on $1, 2, \dots, d = 5$ input states.

Each estimated process is the average of the five reconstructed process matrices, each based on the data associated with an informationally complete measurement record on the five states $|\psi_n\rangle$, $n = 0, 1, \dots, 4$, of Eq. (20), taken in cyclic permutations. The plots on the top and bottom rows correspond to different levels of coherent and incoherent errors. When the prior assumptions are valid and we are in a regime of a low error magnitude (either coherent or incoherent), e.g., $F(\chi_t, \chi_a) = 0.97 \pm 0.005$ in these simulations, the three estimators yield reconstructions with high fidelity to the applied map (and with the target map). While the CS_{Tr} and the LS estimators require d UIC input states to reliably characterize the applied map, with proper formulation, the CS_{ℓ_1} estimator returns a reliable estimate with information obtained from a single input state.

As the error magnitude increases, our prior assumptions become less and less valid, and consequently the estimators yield lower fidelity with the data obtained from of order d input states. The data suggest that with high confidence the following conclusions hold. First, the value of the fidelity $F(\hat{\chi}, \chi_t)$ obtained from d UIC input states serves to validate that the applied map was close to a known target unitary map; the value of $F(\hat{\chi}, \chi_t)$ decreases when the applied map is further from the target. Second, if the error in the applied map is not small, we can infer the dominant source of the imperfection by examining the behavior of the different estimators. As seen in Fig. 3(a), with $F(\chi_t, \chi_a) = 0.83 \pm 0.005$, when employing the CS_{ℓ_1} estimator, a large coherent error results in a curvature in $F(\hat{\chi}, \chi_t)$ as a function of the number of input states. Additionally, for the same data, using the CS_{Tr} and LS estimators, we see that $F(\hat{\chi}, \chi_t)$ exhibits a sharp cusp after d UIC probe states. In contrast, when the errors are predominantly incoherent, we see that when employing the CS_{ℓ_1} estimator, $F(\hat{\chi}, \chi_t)$ is more or less a constant function of the number of input states. In addition, there is a more gradual increase of $F(\hat{\chi}, \chi_t)$ for the CS_{Tr} and LS estimators around d states; the cusp behavior is smoothed. These variations are signatures of the nature of the error in implementing the target unitary map.

In the regime $0.90 \lesssim F(\chi_t, \chi_a) \lesssim 0.97$ it is difficult to distinguish, with high confidence, the nature of errors based solely on the behavior of $F(\hat{\chi}, \chi_t)$ as a function of the input state, and additional methods will be required to diagnose the process matrix. Nonetheless, a low fidelity of $F(\hat{\chi}, \chi_t) \lesssim 0.95$ after d input states challenges the validity of our assumptions and indicates the presence of noise.

VI. SUMMARY AND CONCLUSIONS

We have studied the problem of QPT under the assumption that the applied process is a unitary or close to a unitary map. We found that by probing a unitary map on a d -level system with d specially chosen pure input states (which we called a UIC set of states), one can discriminate it from any other arbitrary CPTP map given the corresponding output states. In the ideal case of no errors, since the latter are completely characterized by a measurement of a POVM with a minimum of $2d$ elements, all together, QPT of a unitary map requires measurement of a total of $2d^2$ POVM elements. This is to be compared with the results of [14] that a measurement of $5d^2 - 3d - 5$ Pauli-like observables

is sufficient to discriminate a unitary map from any other CTPT map, and with $d^4 - d^2$ POVM elements required for discriminating any two arbitrary CPTP map. We then showed that discriminating a unitary map from any other unitary map requires measurements of a minimum number of $d^2 + d$ POVMs elements.

We used the methods for efficient unitary map reconstruction to analyze a more realistic scenario where the applied map is close to a target unitary map and the collected data include statistical errors. Under this assumption, we studied the performance of three convex-optimization-based estimators, the LS, CS_{Tr} , and CS_{ℓ_1} . For each of these estimators we reconstructed the applied process from the same simulated data obtained by probing the map with pure input states, the first d of which form a UIC set. We considered two types of errors that may occur on the target map, coherent errors, for which the applied map is a unitary map but slightly rotated from the target map, and incoherent errors in which the applied map is full rank but with high purity. In our simulation in Sec. V we used the states of Eq. (9) to probe a randomly generated (applied) map with the desired properties.

Our analysis suggests that when the prior assumptions are valid, the three estimators yield high-fidelity estimates with the applied map using only the input UIC set of states. We found that the sensitivity of these methods for various types of errors yields important information about the validity of the prior assumptions and about the nature of the errors that occurred in the applied map. In particular, probing the map with a UIC set of d pure states and obtaining low fidelity between the estimates and the target map indicates that the errors are actually not small and the applied map is not close to the target unitary map. Furthermore, the performance of the different estimators and under coherent and incoherent noise, enables the identification of the dominant error type. One can then take this information into account to further improve the implementation of the desired map.

Further extensions will be necessary before this protocol will be useful in practice. While we have separately studied the effects of coherent and incoherent errors, in any real application both types of error will occur to some degree. We expect that if one error source sufficiently dominates, the signatures we found in the reconstruction that characterize the nature of the error will survive. An additional extension of particular importance is a study of the performance of QPT in the presence of SPAM errors. In the analysis presented here we assumed error neither in the preparation of the probe states nor in the POVM elements measured. Errors of this sort will certainly contaminate the data and make it more difficult to both validate prior assumptions and diagnose errors. Additional analysis is required to calibrate how SPAM errors affect the distinctive signatures of errors in gate implementations.

It is also important to study how the form of the input states that form a UIC set affects our protocol. For example, the information learned from each input state of Eqs. (19) and (20) is qualitatively different, as seen in Fig. 1(a). It is important to design the input states so that the information encoded in the corresponding output state will be as robust as possible. The amplitude $1/\sqrt{2}$ of the states of Eq. (20) was chosen to

ensure robustness against statistical errors. For example, the set of states $\{|0\rangle, \sqrt{0.999}|0\rangle + \sqrt{0.001}|n\rangle, n = 1, \dots, d-1\}$ is UIC, but with large enough statistical errors the information encoded in the $|n\rangle$ states becomes noisy and uninformative. In future work we will examine how the choice of UIC states minimizes the error in the reconstruction due to statistical errors and, perhaps, SPAM errors.

Finally, while the analysis presented in work is inspired by CS methodology, it does not contain all of its elements. In particular, our estimators make use of the sparsity of the process matrix in different bases, depending on the nature of errors and prior information, but we do not make use of the “uniform uncertainty principle,” (UUP) at the heart of

compressive sampling, which ensures that one can substantially reduce data required for high-fidelity reconstruction [26]. It is an important problem to understand how the UUP applies in the context of quantum tomography [20], and thus apply the full methodology of CS to estimate quantum states and processes, validate prior assumptions, and diagnose errors.

ACKNOWLEDGMENTS

We gratefully acknowledge useful discussions with Poul Jessen, Carlos Riofrío, Matthew Grace, and Robert Kosut. This work was supported by NSF Grants No. PHY-1307520 and No. PHY-1212445.

-
- [1] M. A. Nielsen and I. L. Chuang, *Quantum Computation and Quantum Information* (Cambridge University Press, Cambridge, UK, 2000).
- [2] J. Emerson, R. Alicki, and K. Życzkowski, *J. Opt. B* **7**, S347 (2005).
- [3] E. Knill, D. Leibfried, R. Reichle, J. Britton, R. B. Blakestad, J. D. Jost, C. Langer, R. Ozeri, S. Seidelin, and D. J. Wineland, *Phys. Rev. A* **77**, 012307 (2008).
- [4] E. Magesan, J. M. Gambetta, and J. Emerson, *Phys. Rev. Lett.* **106**, 180504 (2011).
- [5] C. A. Ryan, M. Laforest, and R. Laamme, *New J. Phys.* **11**, 013034 (2009).
- [6] J. M. Chow, J. M. Gambetta, L. Tornberg, J. Koch, L. S. Bishop, A. A. Houck, B. R. Johnson, L. Frunzio, S. M. Girvin, and R. J. Schoelkopf, *Phys. Rev. Lett.* **102**, 090502 (2009).
- [7] S. Olmschenk, R. Chicireanu, K. D. Nelson, and J. V. Porto, *New J. Phys.* **12**, 113007 (2010).
- [8] J. P. Gaebler *et al.*, *Phys. Rev. Lett.* **108**, 260503 (2012).
- [9] A. Smith, B. E. Anderson, H. Sosa-Martinez, C. A. Riofrío, I. H. Deutsch, and P. S. Jessen, *Phys. Rev. Lett.* **111**, 170502 (2013).
- [10] R. Barends *et al.*, *Nature (London)* **508**, 500 (2014).
- [11] A. Laing and J. L. O’Brien, [arXiv:1208.2868](https://arxiv.org/abs/1208.2868).
- [12] X.-Q. Zhou, H. Cable, R. Whittaker, P. Shadbolt, J. L. O’Brien, and J. C. F. Matthews, [arXiv:1402.2897](https://arxiv.org/abs/1402.2897).
- [13] D. M. Reich, G. Gualdi, and C. P. Koch, *Phys. Rev. A* **88**, 042309 (2013).
- [14] G. Gutoskia and N. Johnston, *J. Math. Phys.* **55**, 032201 (2014).
- [15] M. A. Davenport, M. F. Duarte, Y. C. Eldar, and G. Kutyniok, in *Compressed Sensing: Theory and Applications* (Cambridge University Press, New York, 2012).
- [16] R. L. Kosut, [arXiv:0812.4323](https://arxiv.org/abs/0812.4323).
- [17] A. Shabani, R. L. Kosut, M. Mohseni, H. Rabitz, M. A. Broome, M. P. Almeida, A. Fedrizzi, and A. G. White, *Phys. Rev. Lett.* **106**, 100401 (2011).
- [18] D. Gross, Y.-K. Liu, S. T. Flammia, S. Becker, and J. Eisert, *Phys. Rev. Lett.* **105**, 150401 (2010).
- [19] Y.-K. Liu, in *Advances in Neural Information Processing Systems (Proceedings of NIPS 2011)*, edited by J. Shawe-Taylor, R. S. Zemel, P. L. Bartlett, F. Pereira, and K. Q. Weinberger (Curran Associates, Inc., Red Hook, NY, 2011), Vol. 24, p. 1638.
- [20] S. T. Flammia, D. Gross, Y.-K. Liu, and J. Eisert, *New J. Phys.* **14**, 095022 (2012).
- [21] K. Hellwig and K. Kraus, *Commun. Math. Phys.* **16**, 142 (1970).
- [22] A. Jamiołkowski, *Rep. Math. Phys.* **3**, 275 (1972); M. D. Choi, *Linear Algebr. Applic.* **10**, 285 (1975).
- [23] J. M. Gambetta *et al.*, *Phys. Rev. Lett.* **109**, 240504 (2012).
- [24] W. K. Wootters and B. D. Fields, *Ann. Phys. (NY)* **191**, 363 (1989).
- [25] Software for disciplined convex programming can found at <http://cvxr.com/>
- [26] E. J. Candès, J. K. Romberg, and T. Tao, *Commun. Pure Appl. Math.* **59**, 1207 (2006).
- [27] E. J. Candès and Y. Plan, *IEEE Trans. Inf. Theory* **57**, 2342 (2011).
- [28] A. N. Korotkov, [arXiv:1309.6405](https://arxiv.org/abs/1309.6405).
- [29] A. Smith, C. A. Riofrío, B. E. Anderson, H. Sosa-Martinez, I. H. Deutsch, and P. S. Jessen, *Phys. Rev. A* **87**, 030102(R) (2013).
- [30] W.-T. Liu, T. Zhang, J.-Y. Liu, P.-X. Chen, and J.-M. Yuan, *Phys. Rev. Lett.* **108**, 170403 (2012).
- [31] S. T. Flammia, A. Silberfarb, and C. M. Caves, *Found. Phys.* **35**, 1985 (2005).
- [32] It was recently shown in [33] that an informationally complete measurement for *all* pure states has at least $4(d-1)$ measurement outcomes.
- [33] T. Heinosaari, L. Mazzarella, and M. M. Wolf, *Commun. Math. Phys.* **318**, 355 (2013).
- [34] W. Bruzda, V. Cappellinia, H.-J. Sommers, and K. Życzkowski, *Phys. Lett. A* **373**, 320 (2009).